Properties and microstructure of alkali-activated red clay brick waste

L. Reig [a], M.M. Tashima [b], M.V. Borrachero [b], J. Monzó [b], C.R. Cheeseman [c], J.Payá [b]

[a] EMC, Universidad Jaume I de Castellón, Av. Sos Baynat s/n 12071 Castelló de la Plana, Spain.

[b] Instituto de Ciencia y Tecnología del Hormigón (ICITECH), Universitat Politècnica de València, Camino de Vera s/n 46022 Valencia, Spain.

[c] Department of Civil and Environmental Engineering, Imperial College London, London SW7 2AZ, UK

Corresponding author: M.V. Borrachero; vborrachero@cst.upv.es

Tel.: +34 96 387 75 64

Fax: +34 96 387 75 69

E-mail address: lreig@uji.es; maumitta@hotmail.com; vborrachero@cst.upv.es; jmmonzo@cst.upv.es; c.cheeseman@imperial.ac.uk; jjpaya@cst.upv.es

Abstract

Sintered red clay ceramic is used to produce hollow bricks which are manufactured in enormous quantities in Spain. They also constitute a major fraction of construction and demolition waste. The aim of this research was to investigate the properties and microstructure of alkali-activated cement pastes and mortars produced using red clay brick waste. The work shows that the type and concentration of alkali activator can be optimised to produce mortar samples with compressive strengths up to 50 MPa after curing for 7 days at 65 °C. This demonstrates a new potential added value reuse application for this important waste material.

Keywords: Ceramic waste (D), Waste Management (E), alkali-activated binder (D), mechanical properties (C).

1. Introduction

Red clay brick waste (RCBW) originating primarily from demolished brick walls represents approximately 54 wt.% of construction and demolition waste in Spain [1]. As previously reported [2], almost 30 million tonnes of structural ceramics and 608 million m^2 of tiles were manufactured by the Spanish ceramics industry in 2006. According to Pacheco-Torgal and Jalali [3], the amount of waste generated by the European ceramic industry is typically 3-7% by weight of total production, suggesting that millions of tonnes of RCBW are generated in Spain each year.

Significant quantities of RCBW are currently used as road sub-base in landscaping and as a coarse aggregate for the production of structural and non-structural concrete [3-5]. The use of sintered clay ceramics as a cementitious material to partially replace Portland cement (PC) clinker has also been investigated. The manufacture of Portland cement requires high amounts of energy (850 kcal per kg of clinker) and involves the emission of typically 0.8-1 Tonne of CO_2 per Tonne of clinker produced [6]. Different alternatives have been proposed to reduce the environmental impact of cement and these include reusing waste materials to produce low-CO_2 cement binders. In the study by Puertas et al. [6,7] ceramic waste materials were used to produce PC clinker, while other studies [3,8,9] investigated the potential of clay ceramics as a supplementary cementitious material. While only a portion of cement is replaced in these applications (usually 10–35 %), binders based on alkali-activation can be produced entirely or almost entirely from waste materials. In alkali-activation reactions alumino-silicate minerals are dissolved by a highly alkaline solution prior to precipitation reactions that form a gel binder [10]. The gel formed by alkali-activation of sintered clay is generally a zeolite precursor containing tetrahedral SiO_4 and AlO_4^- in randomly distributed polymeric chains, cross-linked by bridging oxygen atoms. The negative charge on the AlO_4^- group is balanced by alkali metal cations, typically Na^+ and/or K^+ [11-13].

The use of alumino-silicate minerals such as metakaolin, ground blast furnace slag and fly ash to produce alkali-activated cements has been extensively reported [12,14-17] and there is increasing interest in investigating the suitability of using other materials. Different wastes containing silica and alumina, such as hydrated-carbonated cement [18], glass [19], fluid catalytic cracking catalyst residues (FCC) [20] and waste ceramic materials [21,22] have been alkali-activated. In the work by

Puertas et al. [21], ceramic wastes were activated using NaOH and sodium silicate solution. Although compressive strengths between 7 and 13 MPa were achieved, it was concluded that further research was required to understand the influence of process parameters on the final properties of the binders developed.

This research aimed to optimise alkali-activation of RCBW and understand the influence of the type and concentration of alkali activator used on the mechanical strength and microstructure of the binders formed.

2. Experimental

2.1. Materials

As-received RCBW was crushed to give a granular material with particles less than 4 mm in diameter. This was dry milled using a porcelain ball mill with alumina milling media for 40 minutes to increase the specific surface area [22]. The particle size distribution of milled RCBW shown in Fig. 1 was determined using laser diffraction (Mastersizer 2000, Malvern Instruments). This indicates a mean particle size of approximately 20.9 μm, a d_{90} (90% of volume less than this size) of 56.2 μm and a d_{10} value of 1.2 μm.

The chemical composition of milled RCBW shown in Table 1 was determined by x-ray fluorescence (XRF). RCBW contains high levels of SiO_2 and Al_2O_3, which are essential for alkali-activation, together with moderate amounts of CaO and MgO. The amorphous content, determined following UNE EN 196-2, was around 35%, which is close to that obtained by Puertas et al. [21] for waste red clay tiles. According to Baronio and Binda [23], the amorphous content of bricks sintered between 800 ºC and 1000ºC [9] originates at temperatures between 600°C and 900°C, due to loss of the combined water in clay minerals, which causes breakdown of the crystalline clay network, with the silica and alumina forming a disordered, amorphous phase. Pereira-de-Oliveira et al. [9] report that the amorphous content determines the degree of pozzolanic activity.

The mineralogical composition of RCBW was determined by x-ray diffraction (XRD, Philips diffractometer PW1710 with Cu K_α radiation, 40 kV and 20 mA, 2θ from 5-55º). The data in Fig. 2 shows that quartz (SiO_2) is the major crystalline phase. Albite ($NaAlSi_3O_8$), calcite ($CaCO_3$), anorthite ($CaAl_2Si_2O_8$) and sanidine ($(K,Na)(Si,Al)_4O_8$) were also present as minor constituents [3,8,21]. The particle morphology of milled RCBW was examined using scanning electron microscopy (SEM, JEOL JSM-6300) and this indicates mainly irregularly shaped particles as shown in Fig. 3.

Sodium hydroxide pellets (98% purity, Panreac), water and sodium silicate (Merck, SiO_2=28%, Na_2O=8%, H_2O=64%) were used to prepare alkali-activating solutions.

2.2. RCBW paste and mortar sample preparation

The alkaline activating solutions were prepared by dissolving NaOH pellets in water and adding the required amount of sodium silicate solution. The concentration of Na^+ provided by NaOH and sodium silicate ranged from 2.5 to 10 molal ($mol.kg^{-1}$).

Table 2 summarizes the mix proportions investigated in this research. Mixes are coded 'w/m/r', where w is the amount of water per 100g of RCBW, m is the molality of Na^+ in the activating solution and r is the SiO_2/Na_2O molar ratio in the activating solution.

Alkali-activated RCBW paste samples were obtained by mixing ground RCBW with the required alkaline solution for 4 minutes. Samples were cast in plastic containers, sealed and stored in a thermostatically controlled bath at 65 °C.

Alkali-activated RCBW mortar samples were prepared by mixing RCBW with activating solution for 2 minutes. Siliceous sand (4.36 modulus fineness with maximum particle diameter of 2 mm) was then added using sand/RCBW ratios of 3/1 and 2/1, as shown in Table 2. Mixing continued for a further 3.5 minutes and the mortar samples formed were then placed in a mould and vibrated for 4 minutes. Samples were stored at 65 ºC at a relative humidity of 90-95% for 3 and 7 days.

2.3. Sample testing

The compressive strengths of alkali-activated RCBW mortar samples were determined following UNE EN 196-1. The porosity of the mortars was evaluated by mercury intrusion porosimetry (MIP, AutoPore IV 9500) using pressures between 2 psia (13782Pa) to 32989 psia (227.4 MPa), equivalent to pores with diameters ranging from 91.2 microns to 5.5 nm. Pressures were converted to equivalent pore widths using the Washburn equation, assuming a contact angle of 130º.

The microstructure of RCBW paste samples was examined using SEM-EDX (JEOL JSM-6300). X-ray diffraction (XRD) was used to identify mineralogical phases (Philips diffractometer PW1710 with Cu K_α radiation, 40 kv and 20 mA, 2θ from 5-55º). Fourier transformed infrared spectroscopy (FTIR) analysis of the nanostructure of the materials obtained was conducted with a Mattson Genesis II spectrometer. The KBr pellet method was used to prepare the samples, with spectra collected in transmittance mode from 1500 to 400 cm^{-1}.

Thermogravimetry (TG, 850 Mettler-Toledo) was used to investigate weight loss of samples under a N_2 atmosphere, using sealed pin holed aluminium crucibles at a heating rate of 10 ºC min^{-1}, from 35 ºC to 600 ºC. Samples were analyzed after 3 and 7 days of curing at 65 ºC (relative humidity 90-95%). Samples for TG and XRD analyses were crushed using a pestle and mortar and passed through a 125 µm sieve. Hydration reactions were inhibited by immersing samples in acetone and then placing them in the oven at 60ºC for 30 minutes.

3. Results and discussion

3.1. Compressive strength

3.1.1. Effect of NaOH concentration

Fig. 4 shows the effect of NaOH concentration (molality: 2.5, 5, 7 and 10) on the compressive strength of RCBW mortars prepared at a constant water to binder (w/b) ratio of 0.45. The best alkali-activated samples were obtained using 5.0 molal NaOH ('45/5.0/0.0') after curing for 7 days, while the mechanical properties decreased significantly for higher concentrations of NaOH. This concentration

is close to the optimum established by Puertas et al. [21] who also showed that mechanical properties did not exhibit significant differences when the type or amount of activator was varied. The existence of an optimum concentration was previously reported by Palomo et al. and Tashima [24, 25] for alkali-activated fly ash and vitreous calcium silico-aluminates, respectively. According to Barbosa et al. [26], the optimum concentration of activator depends on the precursor, and must be sufficient to balance the charges of the Si and Al tetrahedral, without providing an excess of NaOH, that may cause the formation of carbonate salts resulting from atmospheric carbonation.

3.1.2. Influence of SiO_2/Na_2O ratio

Fig. 5 shows the compressive strengths of RCBW mortars prepared using a constant 5 molal NaOH concentration with different SiO_2/Na_2O molar ratios (0.73, 1.46, 1.60), for samples cured at 65 ºC for 3 and 7 days. The compressive strength increases as the amount of sodium silicate increased. However, higher silicon contents increased the mortar viscosity and reduced setting time. It was impossible to produce mortars with a SiO_2/Na_2O molar ratio higher than 1.60 for samples with 5 molal NaOH because these samples set within a few seconds of mixing. Results are in agreement with previous studies [20,25,27] where compressive strength generally increase with the addition of more activator. According to Pacheco-Torgal et al. [11], this is due to the presence of sodium silicate in the activating solution which increases the Si/Al ratio, accelerating the geopolymerization process. Provis et al. [27] used dilatometry measurements to prove that the optimum amount of silica depends on the precursor, and must be appropriate to form a highly cross-linked alumino-silicate network and avoid the presence of unreacted silica.

3.1.3 Influence of Na concentration for a constant SiO_2/Na_2O ratio

Fig. 6 summarises the compressive strength data of mortars with a constant SiO_2/Na_2O molar ratio (1.60) and different sodium concentrations, cured at 65 ºC for 3 and 7 days. Although the compressive strength remained almost the same after curing for 3 days for all mortars (14-17 MPa), the mix prepared using 7 molal Na^+ exhibited good workability and gave the highest strengths of 28 MPa after 7 curing days. These results are consistent with previous studies in which the compressive strength was found to depend not only on the SiO_2/Na_2O ratio but also on the activator/binder ratio [17,28,29].

This is related to the optimum concentration of activator for the RCBW. As discussed in sections 3.1.1 and 3.1.2, the Na^+ concentration increases as the sodium silicate content is increased in the alkali-activating solution.

3.1.4 Influence of water/binder (w/b) ratio

The effect of w/b ratio for different Na concentrations on compressive strength is summarized in Fig. 7. For the lowest w/b mixes (except '30/7.0/2.00') the amount of Na^+ and SiO_2 with respect to the RCBW was constant and equal to those prepared for mix '45/7.0/1.60' at 3.15 mol of Na^+ and 2.52 mol of SiO_2 per kg of ceramic waste. Consequently, the concentration Na^+ in the solution increased for mixtures with w/b ratio of 0.40 (8 molal) and 0.35 (9 molal). Two main results are observed. The compressive strength increases as the w/b ratio decreases when the activator/binder and SiO_2/Na_2O ratios are kept constant ('45/7.0/1.60', '40/8.0/1.60', '35/9.0/1.60'). According to Lampris et al. [17], this implies that a 0.35 w/b ratio provides sufficient water to effectively wet all the grains of the source material, which react with the activating solution. As observed by Komnitsas et al. [30], the reduction in compressive strength when the water volume is increased is due to the water not being consumed during hydration resulting in increased porosity.

For every concentration of Na^+, the compressive strength increased as the w/b ratio decreased ('45/8.0/1.60' - '40/8.0/1.60'; '45/9.0/1.60' - '35/9.0/1.60'). This effect was observed after both 3 and 7 days curing, and means that reduced amounts of reagents were used at lower w/b ratios. This is an important result from both an environmental and economic point of view, because the compressive strength increased while reducing the Na^+/binder and SiO_2/binder ratios.

The binder/sand ratio (b/s) was modified in sample '30/7.0/2.00' in order to increase the workability of the fresh mortar and this allowed the SiO_2/Na_2O ratio to be increased to 2.0. A significant improvement in compressive strength was observed, especially for samples cured for 3 days (42.3 MPa), when compared to sample '45/7.0/1.60', which gave the best results with a w/b ratio of 0.45. For this mix, with the lowest w/b ratio, only 2.1 mol of Na^+ and 4.2 mol of SiO_2 were used per kilogram of RCBW. It can be concluded that the amount of water is the dominant parameter in achieving high compressive strengths.

3.2 Mercury intrusion porosimetry

Porosity studies were carried out on selected mortars. These were samples '45/5.0/0.0' and '45/7.0/1.60' with a constant w/b ratio which had the highest compressive strengths for the samples with and without sodium silicate addition.

The total porosity of mortars was reduced when sodium silicate was added to the activating solution: 19.8% for sample '45/5.0/0.0' (without sodium silicate), and 12.0% for sample '45/7.0/1.60' (with sodium silicate). Therefore, higher durability alkali-activated RCBW samples with sodium silicate can be expected due to the reduced ability of aggressive chemical agents to penetrate the microstructure. These values are close to those previously reported for Portland cement pastes and mortars with similar water-to-cement (w/c) ratios. Cook and Hover [31] observed a minimum total porosity of 16.0% for Portland cement paste specimens mixed with a w/c ratio of 0.3 and cured for 56 day, and higher values when increasing the w/c ratio and reducing the curing time (56% for a w/c of 0.7 cured for 1 day). Similar results were reported by Willis et al. [32], who observed a total porosity of 16 and 23% for mortars with a w/c ratio of 0.4 and 0.6, respectively.

Figure 8 shows the pore size distribution for the mortar samples analyzed. There are significant differences between the volume percentages. The capillary porosity was higher for the sample activated with NaOH, with a total volume of 75-80% in the 10nm-1μm range, while this was only 40-45% for the mortar containing sodium silicate. The volume of air voids in the 1-10 μm range was higher for the mortar containing sodium silicate, which could be attributed to the high viscosity of the paste, which allows greater air retention in the mix. These results are contrary to those previously reported by Sindhunata et al. [33], who observed smaller pore sizes with increasing additions of soluble silicate to the activating solution. After analyzing the hydration mechanisms of Portland cement and inorganic polymer pastes, Lloyd et al. [34] also concluded that larger pores may be expected in samples activated without silicate. In Portland cement pastes C-S-H gel grows outwards from the surface of hydrating cement grains, forming ''C-S-H gel" pores 1.5 nm in diameter and ''capillary" pores, which are much larger and are the remains of originally water-filled spaces that have not become filled with C-S-H gel [35]. The growth of C-S-H gel in alkali-activated systems occurs through the sample, which explains the absence of capillary pores, as much of the volume between the

particles fills concurrently with C-S-H gel to form the hardened binder structure. However, in the absence of dissolved silicate the mechanism of inorganic polymer gel formation is more similar to that of Portland cement, i.e. growth of reaction products outwards from the surface of the binder grains, and therefore capillary pores may be expected in samples activated only with NaOH. However, it was observed that, unlike the capillary pores present in Portland cement pastes, these pores were separated by regions of C-S-H gel. Access to these pores, via the smaller pores of the gel, would cause a pronounced ‘‘ink bottle” effect. Consequently, the MIP results may be misrepresenting the pore size distribution [32,33,35]. This is because the pore size measurement in based on the diameter of access throat through which the mercury penetrates the pore.

3.3 Thermogravimetric analysis

Table 3 shows thermogravimetric analysis data giving the total weight loss of pastes cured for 3 and 7 days. A general increase in water loss with curing time is observed, which may be associated with a greater degree of alkali-activation [20]. Weight loss generally increases with Na^+ concentration which, according to Bernal et al. [36], can be related to a higher degree of chemically bounded water and OH^- groups, provided by NaOH, in the binding phase. Samples with the same SiO_2/Na_2O ratio (1.60) gave similar thermogravimetric loss without a specific trend. The reduction in the w/b ratio did not decrease the total weight loss, suggesting that the water molecules and OH^- groups bonded to the geopolymer matrix are not related to the initial mix water.

As observed in Fig. 9, all paste samples showed a peak weight loss between 120 and 150 ºC which, according to several authors [20,25, 36], is attributed to free or loosely bound water present in these samples. As shown in Fig. 9a, among the pastes activated without sodium silicate, only sample ‘45/5.0/0.0’ presented two peaks in the DTG curve. Although Stakebake [37] associated the second peak centred at 185 ºC to a weight loss from zeolitic phases, these could not be clearly identified by XRD. In the studies performed by Bernal et al. [36] signals related to zeolitic reaction products could not be distinguished by thermogravimetry, because they tend to show a broad dehydration peak in the same temperature range attributed to the loosely bound water present in the samples (60-160 ºC).

Thermogravimetric data for alkali-activated RCBW paste samples using sodium hydroxide and sodium silicate are shown in Fig. 9b. These tend to have a broader first peak when the amount of reagents is increased. The second peak can only be clearly distinguished for lower SiO_2/Na_2O ratio paste (0.73), and it progressively overlaps with the first peak when the concentration of the solution is increased. According to Duxson et al. [13], this is because zeolitic-like phases are less likely to form in highly concentrated solutions due to increased difficulties in phase transport and reorganization.

3.4 X-ray diffraction studies

Fig. 10 shows XRD diffraction data for pastes '45/5.0/0.0' and '45/7.0/1.60', after curing for 7 days at 65 ºC. The XRD data for the as-received RCBW is shown for comparison. The quartz phase was found to be largely unreactive [12], and remained in the sample after the alkali-activation process. Paste '45/5.0/0.0' showed a peak that did not appear in the raw material, denoting the formation of natrite (N, Na_2CO_3). This did not appear in samples prepared with sodium silicate. Results are in agreement with thermogravimetry data reported by Provis et al. [27], who observed that silicate-activated samples presented low mass loss between 200 ºC and up to approximately 800 ºC. However, hydroxide-activated samples showed an additional mass loss, which was attributed to the decomposition of carbonates, resulting from atmospheric carbonation formed during the preparation of the samples prior to analyses. Bernal et al. [36] attributed the DTG peaks observed at temperatures between 650 °C and 670 °C and 770 to 790 °C to carbonates.

Previous studies [12,13] have demonstrated that crystalline phases are less likely to form when sodium silicate solutions are used because high SiO_2 concentrations confer greater stability to the amorphous phases. Despite authors such as Duxson et al. [13] and Criado et al. [28] having noted the formation of semi-crystalline to crystalline phases from the geopolymeric gel, usually zeolitic in nature, these could not be clearly identified in these samples.

3.5 Scanning electron microscopy

Fracture surfaces of alkali-activated RCBW pastes are shown in Fig. 11. RCBR particles can be observed, indicating that some larger particles had only partially reacted during alkali-activation as

complete reaction depends on the particle size. This has led to the development of different morphologies, giving rise to a heterogeneous microstructure containing unreacted ceramic waste particles surrounded by alkali-activation reaction products. It seems that smaller particles were completely dissolved by the alkali solution, while the larger ones are only partially reacted. The strengthening or weakening effect will depend on whether the particles themselves are strong or weak, and also whether they are bonded on the surfaces to the matrix. Studies performed by Yungsen et al. [38] showed that the unreacted particles reduced the compressive strength while Kourti et al. [19] found that unreacted glass could increase strength and toughness.

As expected from XRD results, crystalline phases were developed in samples with 10 molal Na^+ as shown in Fig. 11b. EDX analysis confirmed the high concentration of Na^+ had produced sodium carbonate (natrite) by atmospheric carbonation [39]. This, together with the mechanical properties obtained, confirmed that this concentration of activator was in excess for this sample and this is deleterious to the alkali activation process [17]. Although the development of crystalline phases was observed in some samples as in Fig. 11d, these could not be clearly identified by XRD.

3.6 Fourier transformed infrared spectroscopy (FTIR)

Infrared spectra of the as-received RCBW and pastes '45/5.0/0.0' and '45/7.0/1.60', cured for 7 days at 65 ºC, are shown in Fig. 12. The spectra obtained were normalized in order to allow direct comparison between them. The presence of unreacted particles, previously observed by SEM and XRD, was corroborated by FTIR. According to Criado et al. [28], the quartz gives rise to a series of bands located at 1145, 1084, 796-778, 697, 668, 522 and 460 cm^{-1} in the IR spectrum. Although these bands persist after activation, a reduction in intensity is observed, which indicates that quartz has partially reacted. The higher reduction observed for the sample containing soluble silica ('45/7.0/1.60') implies greater reactivity, which leads to further development of the alkali-activation reaction products. These results are consistent with the lower porosity and improved compressive strength presented by the samples alkali-activated with sodium silicate.

A wide and intense band appears from 950 cm^{-1} to ~1200 cm^{-1}. The interpretation of this region may be difficult, as bond vibrations of different compounds tend to overlap, producing a highly complex

spectrum. While in the unreacted RCBW this band appears at ~1045 cm^{-1}, in the activated samples it shifts to lower wave numbers (~1011 cm^{-1}). According to authors such as Rees et al. [40] and Hajimohammadi et al. [41], this shift occurs due to the formation of aluminosilicate gel, as the asymmetric stretching vibrations of the newly formed Si-O-T (T = Al, Si) bonds originate a new band growing at 960 cm^{-1}. Although a gel with a higher Si/Al ratio is expected for the '45/7.0/1.60' sample, the nature of the gel formed could not be clearly distinguished from FTIR results, due to the Al-enriched gel phase band (~1020 cm^{-1}, from [41]), and the primary band of the Si-O-T bonds in the gel overlap. Furthermore, the bands associated with the vitreous phases of the raw material were also expected to appear in this region (950 cm^{-1} to 1100 cm^{-1} [28]). Although they could not be distinguished, the intensity was expected to decrease as the alumino-silicate gel formation proceeded.

The bands appearing at 871 cm^{-1} and 1415 cm^{-1} in the raw material spectrum are associated with pure $CaCO_3$ [42], attributed to out-of-plane deformation and asymmetric stretching vibrations, respectively. Both bands shift to higher wave numbers after the activation process which, according to Zaki et al. [43] relates to CO_3^{2-} impurity species. This, together with the higher intensity of the peaks appearing in the spectrum of the sample activated with only NaOH ('45/5.0/0.00'), correlates well with XRD and SEM results, where the presence of Natrite (Na_2CO_3) was observed.

No definite peaks were observed in the regions highlighted by Rees et al. [44] as zeolite characteristic regions. This is in good agreement with XRD results, and confirms that it is unlikely that the system contains significant quantities of zeolite nanocrystals.

4. Conclusions

This research has demonstrated that red clay brick waste (RCBW) can form alkali-activated cement pastes and mortars using NaOH and sodium silicate solution as activators. Although thermogravimetric analysis identified initial formation of zeolitic structures, these tend to disappear when the concentration of the alkaline solution increased. The optimum mix was found to be '45/7.0/1.60', and this gave compressive strengths close to 30 MPa after 7 curing days. The mechanical properties were further increased up to 50 MPa by optimising the w/b, b/s and SiO_2/Na_2O ratios.

Acknowledgements

The authors are grateful to the Spanish Ministry of Science and Innovation for supporting this study through Project GEOCEDEM BIA 2011-26947, and to FEDER funding. They also thank the Institute for Science and Technology of Concrete – ICITECH, for providing the means to carry out this investigation; and Universitat Jaume I, for supporting this research through the research stay granted.

References

[1] Ministerio de Fomento de España, Actualización del catálogo de Residuos Utilizables en Construcción, 2010, pp. 123-158.

[2] Reig L, Tashima MM, Soriano L, Borrachero MV, Monzo J, Paya J. Alkaline Activation of Ceramic Waste Materials. Waste Biomass Valor 2013; DOI 10.1007/s12649-013-9197-z.

[3] Pacheco-Torgal F, Jalali S. Reusing ceramic wastes in concrete. Constr Build Mater 2010; 24 (5): 832-838.

[4] Senthamarai RM, Manoharan PD. Concrete with ceramic waste aggregate. Cement Concrete Comp 2005; 27 (9-10): 910-913.

[5] Medina C, Juan A, Frías M, Sánchez-de-Rojas MI, Morán JM, Guerra MI. Characterization of Concrete made with Recycled Aggregate from Ceramic Sanitary Ware. Mater Construcc 2011 [on line] accepted manuscript. DOI: 10.3989/mc.2011.59710.

[6] Puertas F, García-Díaz I, Barba A, Gazulla MF, Palacios M, Gómez MP, Martínez-Ramírez S. Ceramic wastes as alternative raw materials for Portland cement clinker production. Cement Concrete Comp. 2008; 30 (9):798-805.

[7] Puertas F, García-Díaz I, Palacios M, Gazulla MF, Gómez MP, Orduña M. Clinkers and cements obtained from raw mix containing ceramic waste as a raw material. Characterization, hydration and leaching Studies. Cement Concrete Comp 2010; 32 (3):175-186.

[8] Lavat AE, Trezza MA, Poggi M. Characterization of ceramic roof tile wastes as pozzolanic admixture. Waste Manage 2009; 29 (5):1666-1674.

[9] Pereira-de-Oliveira LA, Castro-Gomes JP, Santos PMS. The potential pozzolanic activity of glass and red-clay ceramic waste as cement mortars components. Constr Build Mater 2012;31:197–203.

[10] Davidovits J. 30 Years of Successes and Failures in Geopolymer Applications. Market Trends and Potential Breakthroughs, Geopolymer 2002 Conference 2002; October 28-29, Melbourne, Australia.

[11] Pacheco-Torgal F, Castro-Gomes J, Jalali S. Alkali-activated binders: A review. Part 1. Historical background, terminology, reaction mechanisms and hydration products. Constr Build Mater 2008; 22: 1305-1314.

[12] Yao X, Zhang Z, Zhu H, Chen Y. Geopolymerization process of alkali-metakaolinite characterized by isothermal calorimetry. Thermochim Acta 2009;493:49-54.

[13] Duxson P, Fernández-Jiménez A, Provis JL, Lukey GC, Palomo A, van Deventer JSJ. Geopolymer technology: the current state of the art. J Mater Sci 2007; 42 (9):2917-2993.

[14] Pacheco-Torgal F, Castro-Gomes J, Jalali S. Alkali-activated binders: A review. Part 2. About materials and binders manufacture. Constr Build Mater 2008; 22:1315-1322.

[15] Bernal SA, Mejía de Gutiérrez R, Provis JL. Engineering and durability properties of concretes based on alkali-activated granulated blast furnace slag/metakaolin blends. Constr Build Mater 2012; 33:99-108.

[16] Puertas F, Fernández-Jiménez A. Mineralogical and microstructural characterisation of alkali-activated fly ash/slag pastes. Cement Concrete Comp 2003;25:287–292.

[17] Lampris C, Lupo R, Cheeseman CR. Geopolymerisation of silt generated from construction and demolition waste washing plants. Waste Manage 2009;29:368-373.

[18] Payá J, Borrachero MV, Monzó J, Soriano L, Tashima MM. A new geopolymeric binder from hydrated-carbonated cement. Mater Lett 2012;74:223-225.

[19] Kourti I, Rani DA, Deegan D, Boccaccini AR, Cheeseman CR. Production of geopolymers using glass produced from DC plasma treatment of air pollution control (APC) residues. J Hazard Mater 2010;176:704-709.

[20] Tashima MM, Akasaki JL, Castaldelli VN, Soriano L, Monzó J, Payá J, Borrachero MV. New geopolymeric binder based on fluid catalytic cracking catalyst residue (FCC). Mater Lett 2012;80:50-52.

[21] Puertas F, Barba A, Gazulla MF, Gómez MP, Palacios M, Martínez-Ramírez S. Residuos cerámicos para su posible uso como materia prima en la fabricación de clínker de cemento Portland: caracterización y activación alcalina. Mater. Construcc 2006;56 (281):73-84.

[22] Reig L, Tashima MM, Borrachero MV, Monzó J, Payá J. Nuevas matrices cementantes generadas por Activación Alcalina de residuos cerámicos. II Simposio Aprovechamiento de residuos

agro-industriales como fuente sostenible de materiales de construcción 2010, November 8-9, Valencia, Spain, 199-207.

[23] Baronio G, Binda L. Study of the pozzolanicity of some bricks and clays. Constr Build Mater 1997;11 (1): 41-46.

[24] Palomo A, Grutzeck MW, Blanco MT. Alkali-activated fly ashes: a cement for the future. Cement Concrete Res 1999;29:309-317.

[25] Tashima MM. Produccion y caracterizacion de materiales cementantes a partir del silicoaluminato calcico vitreo (VCAS). Tesis de doctorado, Departamento de Ingeniería de la construcción y de proyectos de ingeniería civil, UPV, 2012.

[26] Barbosa VFF. Sintese e caracterização de polissialatos, Tese de doutorado, Instituto militar de engenharia - IME, 1999.

[27] Provis JL, Harrex RM, Bernal AS, Duxson P, Deventer JSJ. Dilatometry of geopolymers as a means of selecting desirable fly ash sources. J non-cryst solids 2012;358:1930–1937.

[28] Criado M, Fernández-Jiménez A, Palomo A. Alkali activation of fly ash: Effect of the SiO_2/Na_2O ratio Part I: FTIR study. Micropor Mesopor Mat 2007;106:180–191.

[29] Fernández-Jiménez A, de la Torre AG, Palomo A, Lopez-Olmo G, Alonso MM, Aranda MAG. Quantitative determination of phases in the alkali activation of fly ash. Part I. Potential ash reactivity. Fuel 2006;85:625–634.

[30] Komnitsas K, Zaharaki D, Perdikatsis V. Geopolymerisation of low calcium ferronickel slags. J Mater Sci 2007;42:3073–3082.

[31] Cook RA, Hover KC. Mercury porosimetry of hardened cement pastes. Cement Concrete Res 1999;29:933–943.

[32] Willis KL, Abell AB, Lange DA. Image-based characterization of cement pore structure using Wood's metal intrusion. Cement Concrete Res 1998; 28 (12):1695–1705.

[33] Sindhunata, van Deventer JSJ, Lukey GC, Xu H. Effect of curing temperature and silicate concentration on Fly-Ash-based geopolymerization. Ind Eng Chem Res 2006;45:3559-3568.

[34] Lloyd RR, Provis JL, van Deventer JSJ. Microscopy and microanalysis of inorganic polymer cements. 2: the gel binder. J Mater Sci 2009;44:620–631.

[35] Lloyd RR, Provis JL, Smeaton KJ, van Deventer JSJ. Spatial distribution of pores in fly ash-based inorganic polymer gels visualized by Wood's metal intrusion. Micropor Mesopor Mat 2009;126:32-39.

[36] Bernal SA, Gutierrez RM, Provis JL, Rose V. Effect of silicate modulus and metakaolin incorporation on the carbonation of alkali silicate-activated slags. Cement Concrete Res 2010;40: 898–907.

[37] Stakebake JL. Characterization of Natural Chabazite and 5A Synthetic Zeolites. Part I. Thermal and outgassing properties. J Colloid Interf Sci 1984;99(1):41-49.

[38] Yunsheng Z, Wei S, Qianli C, Lin C. Synthesis and heavy metal immobilisation behaviour of slag based geopolymer. J Hazard Mater 2007;143:206–213.

[39] Komnitsas K, Zaharaki D. Geopolymerisation: A review and prospects for the minerals industry. Miner Eng 2007;20:1261–1277.

[40] Rees CA, Provis JL, Lukey GC, van Deventer JSJ. In Situ ATR-FTIR Study of the Early Stages of Fly Ash Geopolymer Gel Formation. Langmuir 2007;23:9076–9082.

[41] Hajimohammadi A, Provis JL, van Deventer JSJ. Time-resolved and spatially-resolved infrared spectroscopic observation of seeded nucleation controlling geopolymer gel formation. J Colloid Interface Sci 2011;357:384–392.

[42] Tatzber M, Stemmer M, Spiegel H, Katzlberger C, Haberhauer G, Gerzabek MH. An alternative method to measure carbonate in soils by FT-IR spectroscopy. Environ Chem Lett 2007;5:9–12.

[43] Zaki MI, Knözinger H, Tesche B, Mekhemer GAH. Influence of phosphonation and phosphation on surface acid–base and morphological properties of CaO as investigated by in situ FTIR spectroscopy and electron microscopy. J Colloid Interface Sci 2006;303:9–17.

[44] Rees CA, Provis JL, Lukey GC, van Deventer JSJ. Attenuated Total Reflectance Fourier Transform Infrared Analysis of Fly Ash Geopolymer Gel Aging. Langmuir 2007;23:8170–8179.

Table

Table 1. Chemical composition of RCBW material.

Oxide	%Wt
SiO_2	49.9
Al_2O_3	16.6
Fe_2O_3	6.5
CaO	9.7
MgO	5.5
Na_2O	0.5
TiO_2	0.8
MnO	0.1
P_2O_5	0.2
SO_3	3.3
K_2O	4.4
Other	0.2
LOI	2.4

Table 2. Mix proportions of alkaline activated mortars.

Mix ('ω/m/r') [#]	w/b	binder/sand, wt	Na^+, m	SiO_2/Na_2O, r
45/2.5/0.0	0.45	1:3	2.5	0.00
45/5.0/0.0	0.45	1:3	5.0	0.00
45/7.5/0.0	0.45	1:3	7.5	0.00
45/10.0/ 0.0	0.45	1:3	10.0	0.00
45/5.0/0.73	0.45	1:3	5.0	0.73
45/5.0/1.46	0.45	1:3	5.0	1.46
45/5.0/1.60	0.45	1:3	5.0	1.60
45/6.0/1.60	0.45	1:3	6.0	1.60
45/7.0/1.60	0.45	1:3	7.0	1.60
45/8.0/1.60	0.45	1:3	8.0	1.60
45/9.0/1.60	0.45	1:3	9.0	1.60
40/8.0/1.60	0.40	1:3	8.0	1.60
35/9.0/1.60	0.35	1:3	9.0	1.60
30/7.0/2.00	0.30	1:2	7.0	2.00

[#] 'ω/m/r' means "water / sodium molality / (SiO_2/Na_2O) activator molar ratio"

Table 3. Thermogravimetric total loss of weight in RCBW pastes cured at 65°C

Sample	Weight loss at different Curing Ages	
	3 days	7 days
45/2.5/0.0	3.41	3.49
45/5.0/0.0	7.26	9.15
45/7.5/0.0	6.51	6.60
45/10.0/ 0.0	7.56	8.34
45/5.0/0.73	6.93	7.63
45/5.0/1.46	5.26	6.77
45/5.0/1.60	5.07	8.99
45/6.0/1.60	6.81	9.99
45/7.0/1.60	6.75	8.62
45/8.0/1.60	7.41	8.09
45/9.0/1.60	7.25	10.26
40/8.0/1.60	7.01	9.84
35/9.0/1.60	7.39	9.84
30/7.0/2.00	7.42	7.86

Figure

CAPTIONS TO ILLUSTRATIONS:

Fig.1. Particle size distribution curve of ground RCBW.

Fig.2. X-Ray diffractogram of raw RCBW material. Q: Quartz (SiO_2); A: Albite ($NaAlSi_3O_8$); An: Anortite ($CaAl_2Si_2O_8$); S: Sanidine ($(K,Na)(Si,Al)_4O_8$); C: Calcite ($CaCO_3$).

Fig.3. SEM micrograph of ground RCBW.

Fig.4. Influence of NaOH solution on compressive strength of alkali activated RCBW mortars cured 3 and 7 days at 65ºC ('ω/m/r' labels in the figures correspond to mix proportions according to Table 2).

Fig.5. Influence of SiO_2/Na_2O molar ratio on the compressive strength, for a constant 5 molal Na^+ concentration ('ω/m/r' labels in the figures correspond to mix proportions according to Table 2).

Fig.6. Influence of sodium concentration on compressive strength development, for a constant SiO_2/Na_2O molar ratio in the activating solution ('ω/m/r' labels in the figures correspond to mix proportions according to Table 2).

Fig.7. Influence of the w/b ratio on compressive strength of alkali activated RCBW mortars ('ω/m/r' labels in the X-axis correspond to mix proportions according to Table 2).

Fig.8. Pore size distribution of samples '45/5.0/0.0' and '45/7.0/1.60', (x-axis labels in micrometers).

Fig.9. Differential thermogravimetric curves for alkali activated RCBW pastes: a) with NaOH solution; b) with NaOH and sodium silicate solution.

Fig.10. X-Ray diffractograms of raw material; '45/5.0/0.0' and '45/7.0/1.60' pastes after curing at 65ºC for 7 days. Q: Quartz; N: Natrite; A: Albite.

Fig.11. Scanning electron microscope images of RCBW alkali activated pastes cured for 7 days at 65ºC: a) 45/5.0/0.0; b) 45/10/0.0, c) 45/9.0/1.60; d) 45/7.0/1.60.

Fig.12. FTIR spectra of RCBW and alkali-activated ‘45/5.0/0.0’ and ‘45/7.0/1.60’ pastes cured at 65ºC for 7 days.

Figure

Click here to download high resolution image

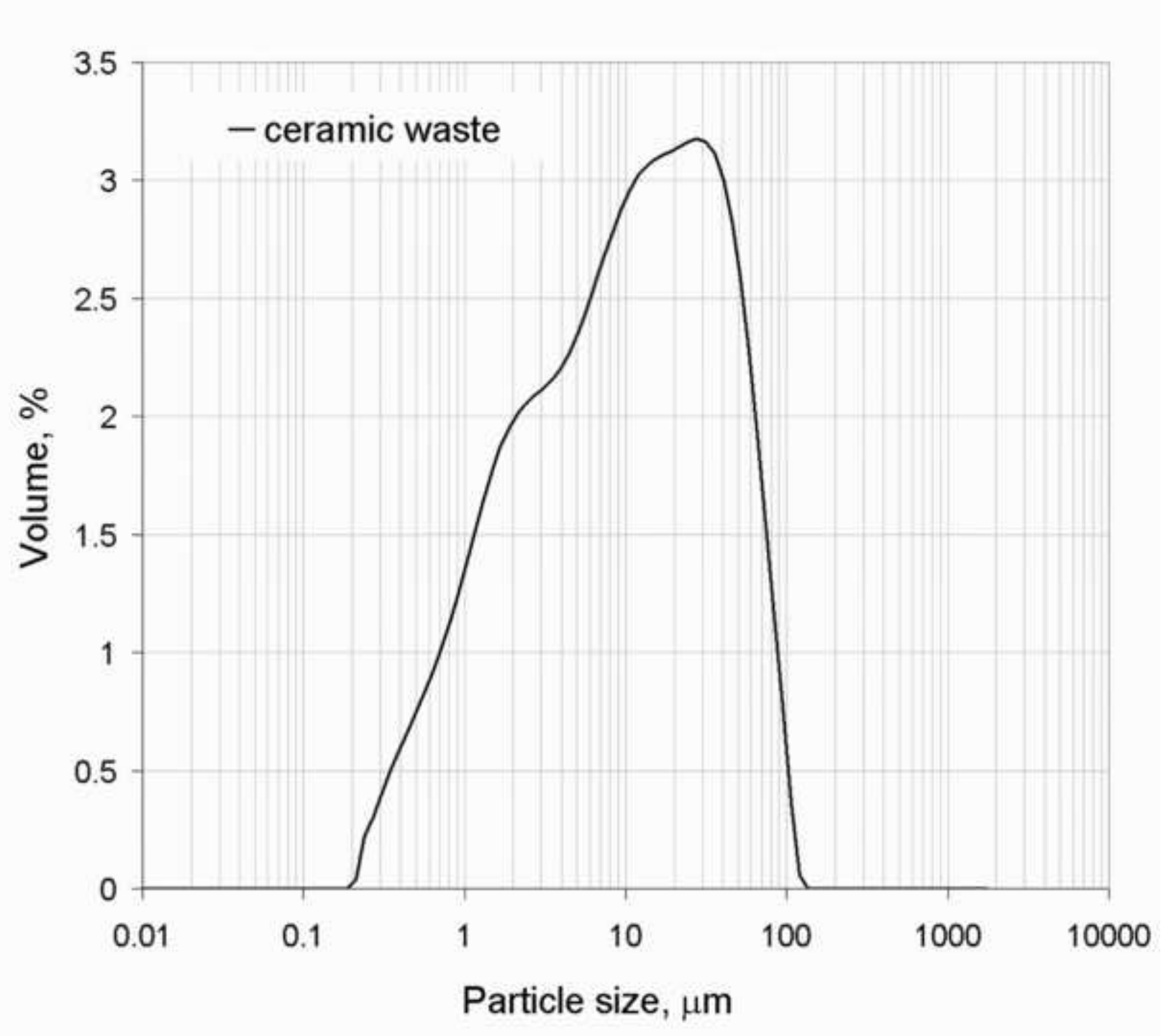

Figure

Click here to download high resolution image

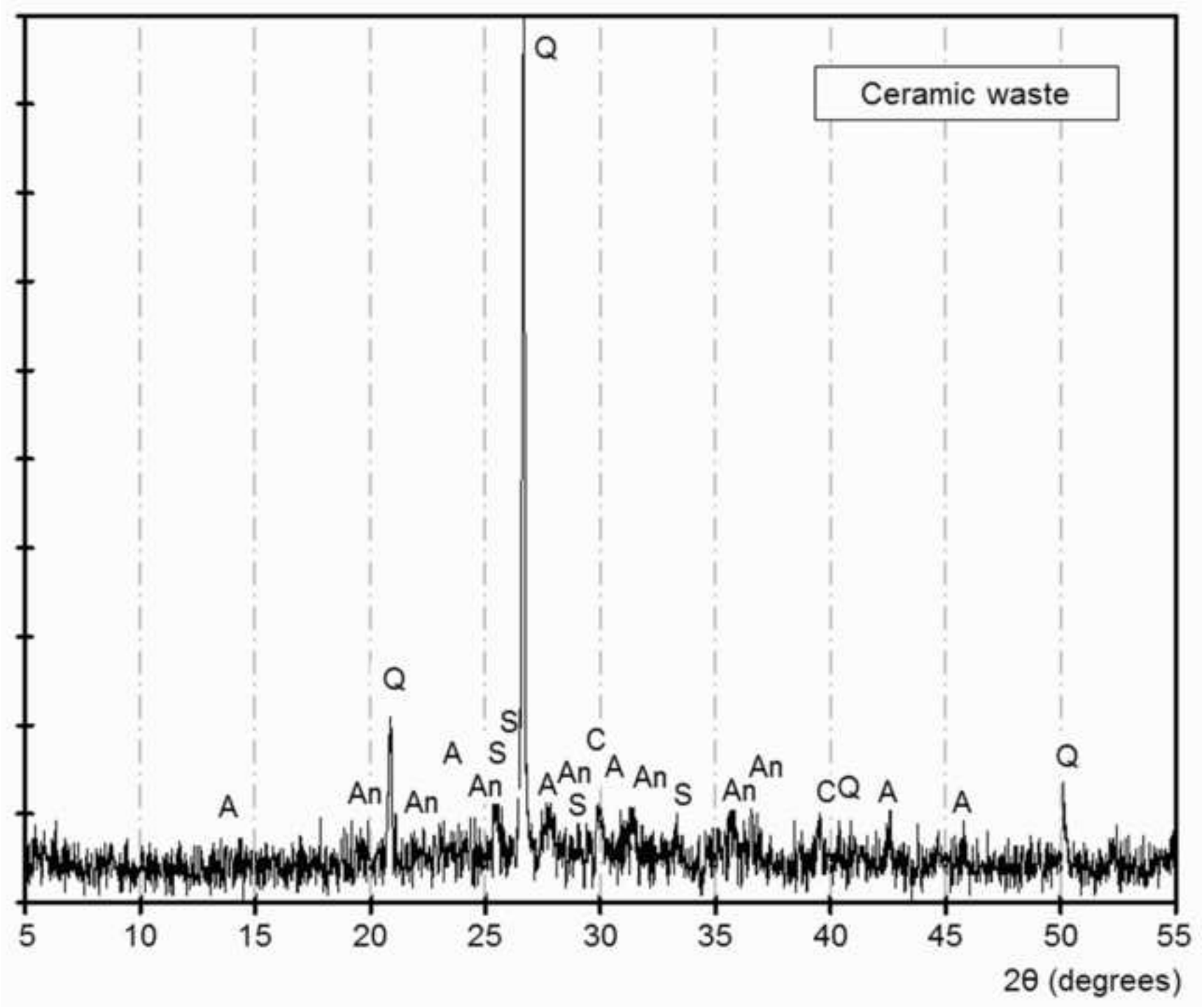

Figure

Click here to download high resolution image

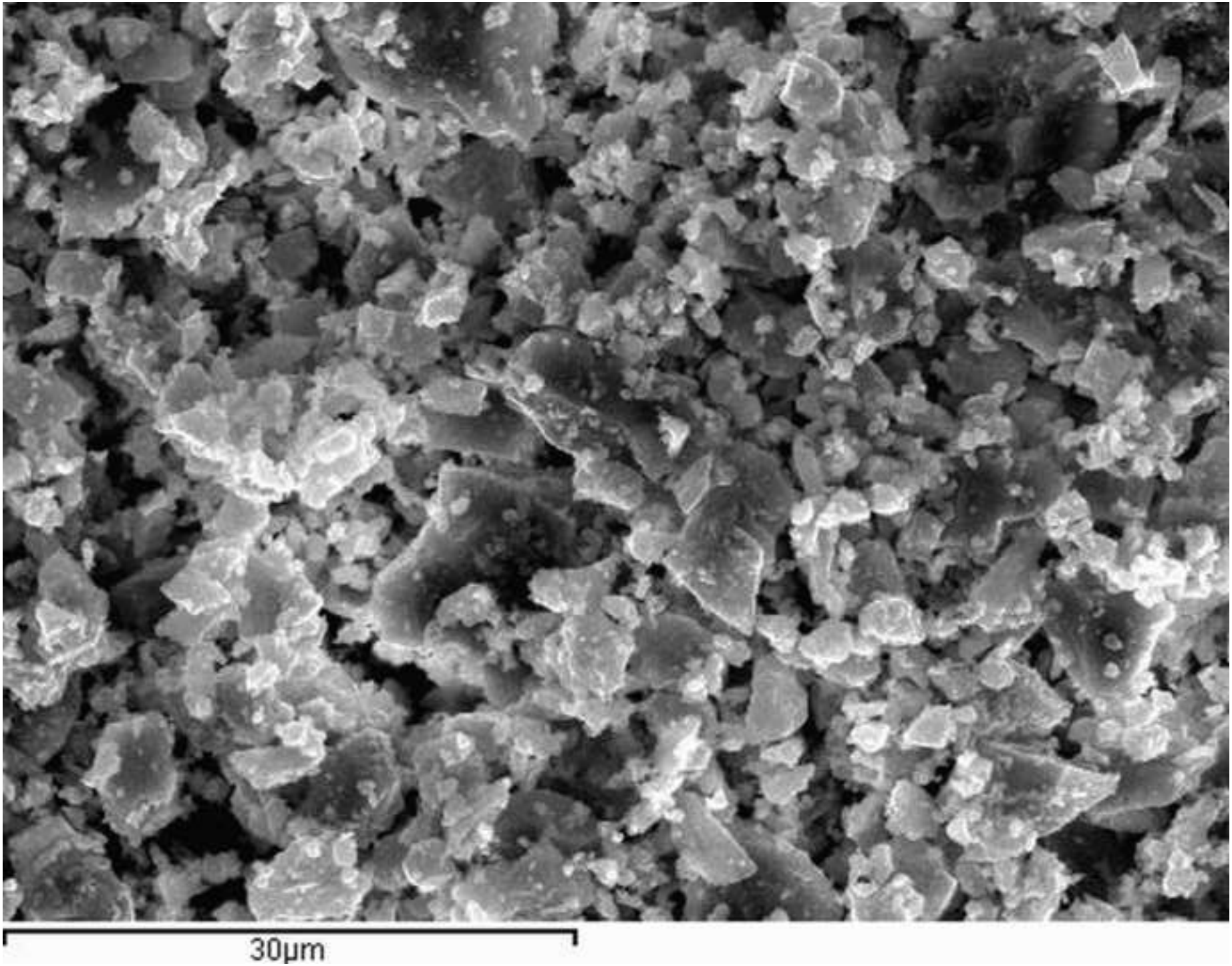

Figure
Click here to download high resolution image

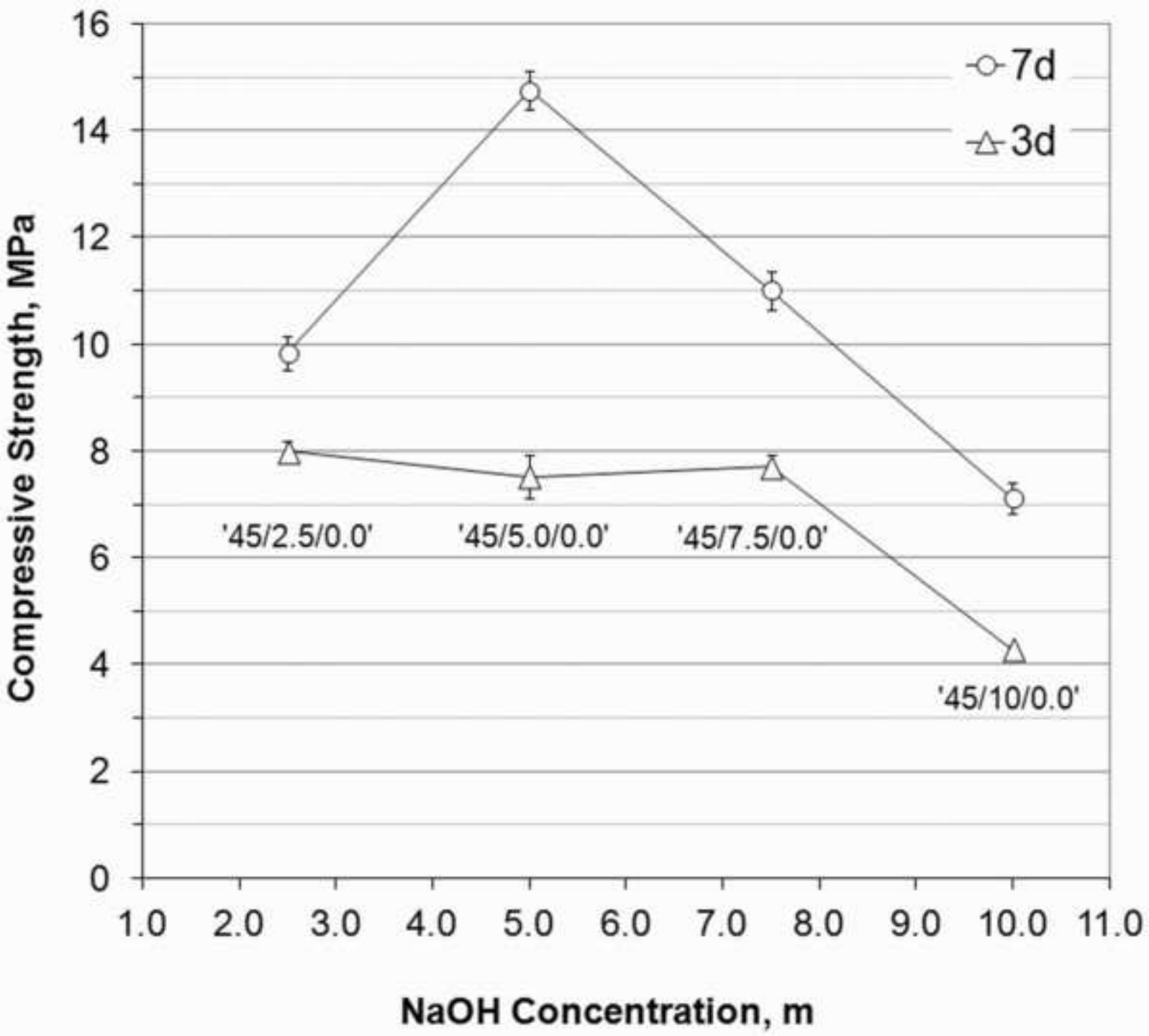

Figure

Click here to download high resolution image

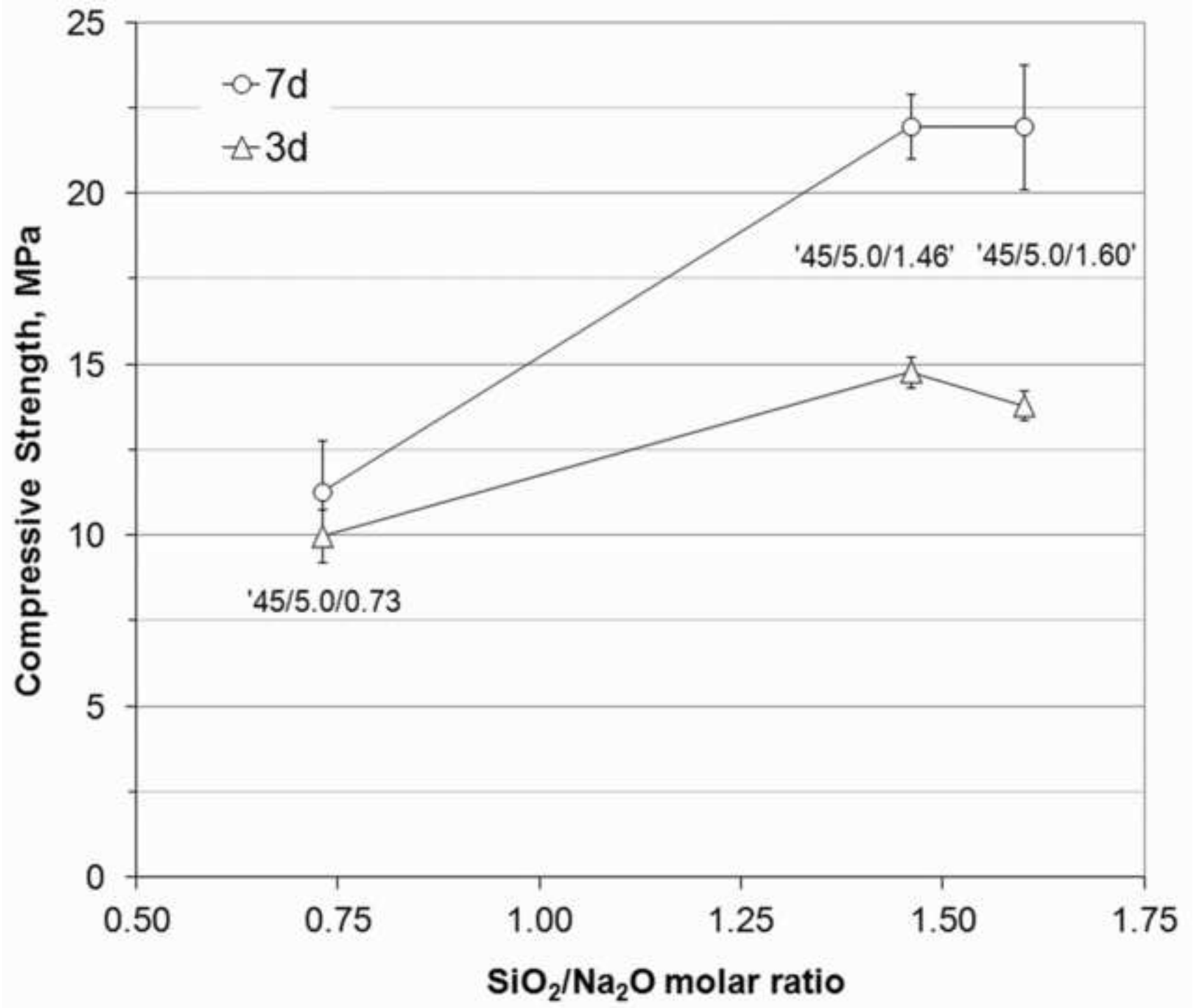

Figure

Click here to download high resolution image

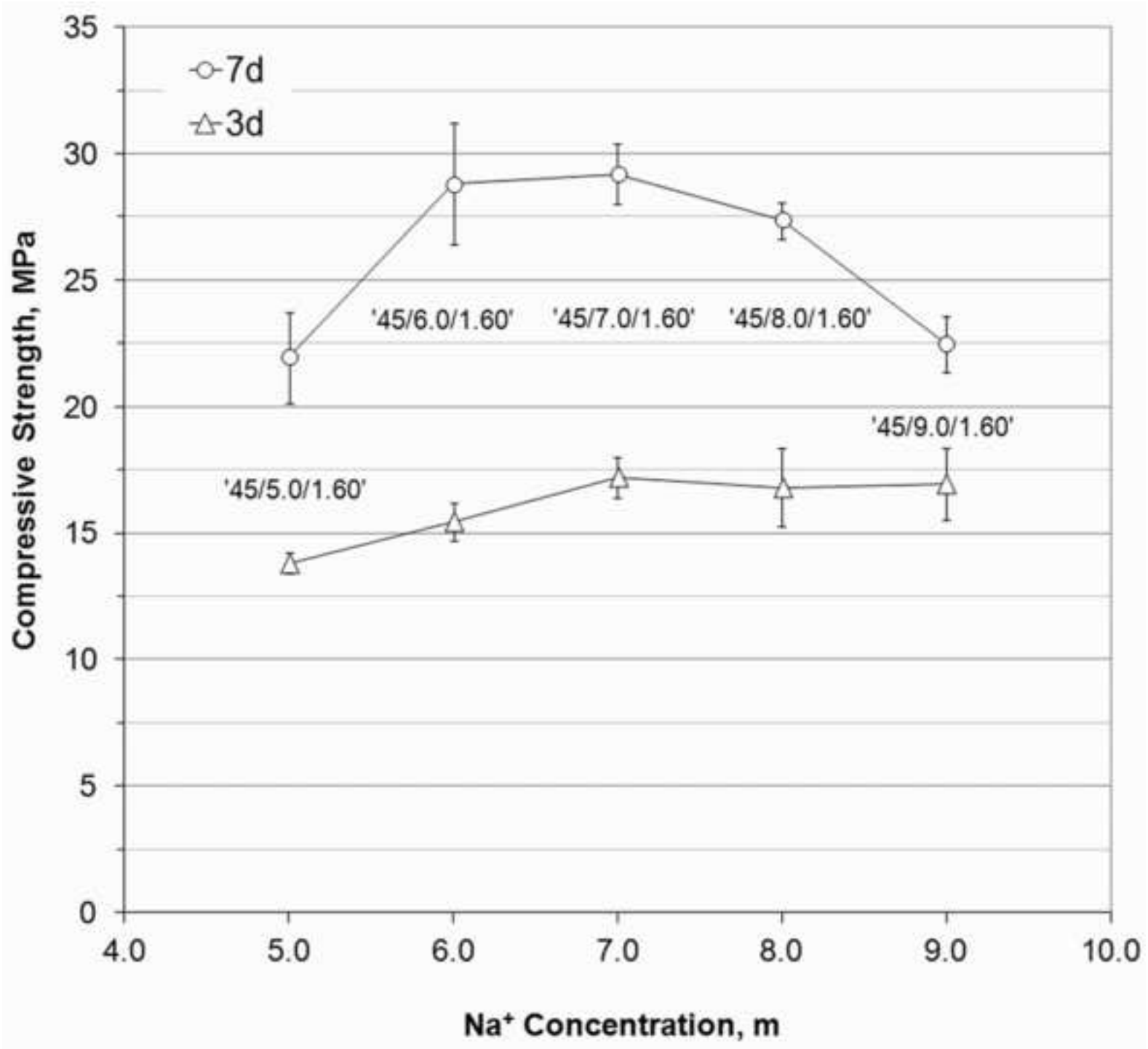

Figure

Click here to download high resolution image

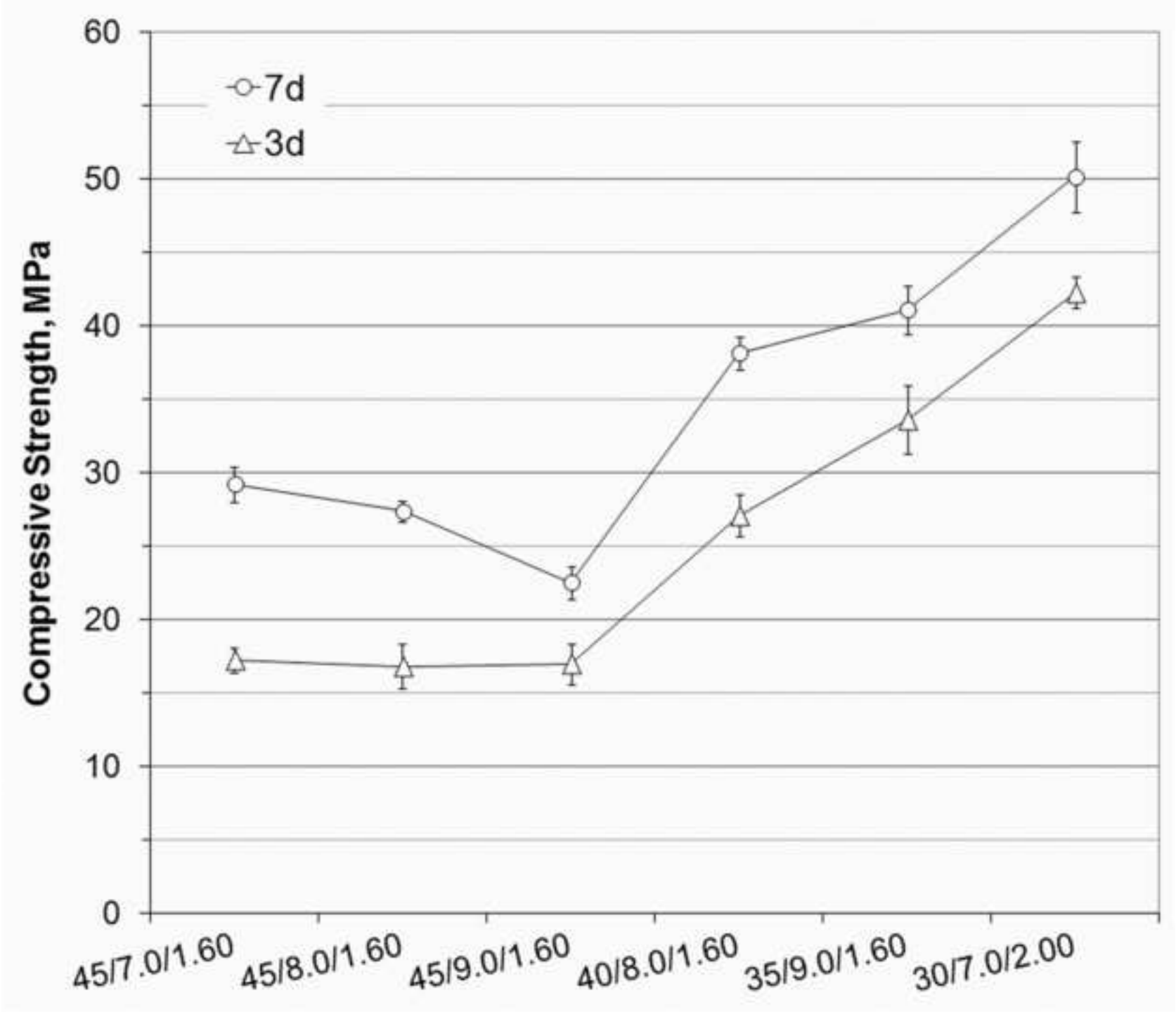

Figure
Click here to download high resolution image

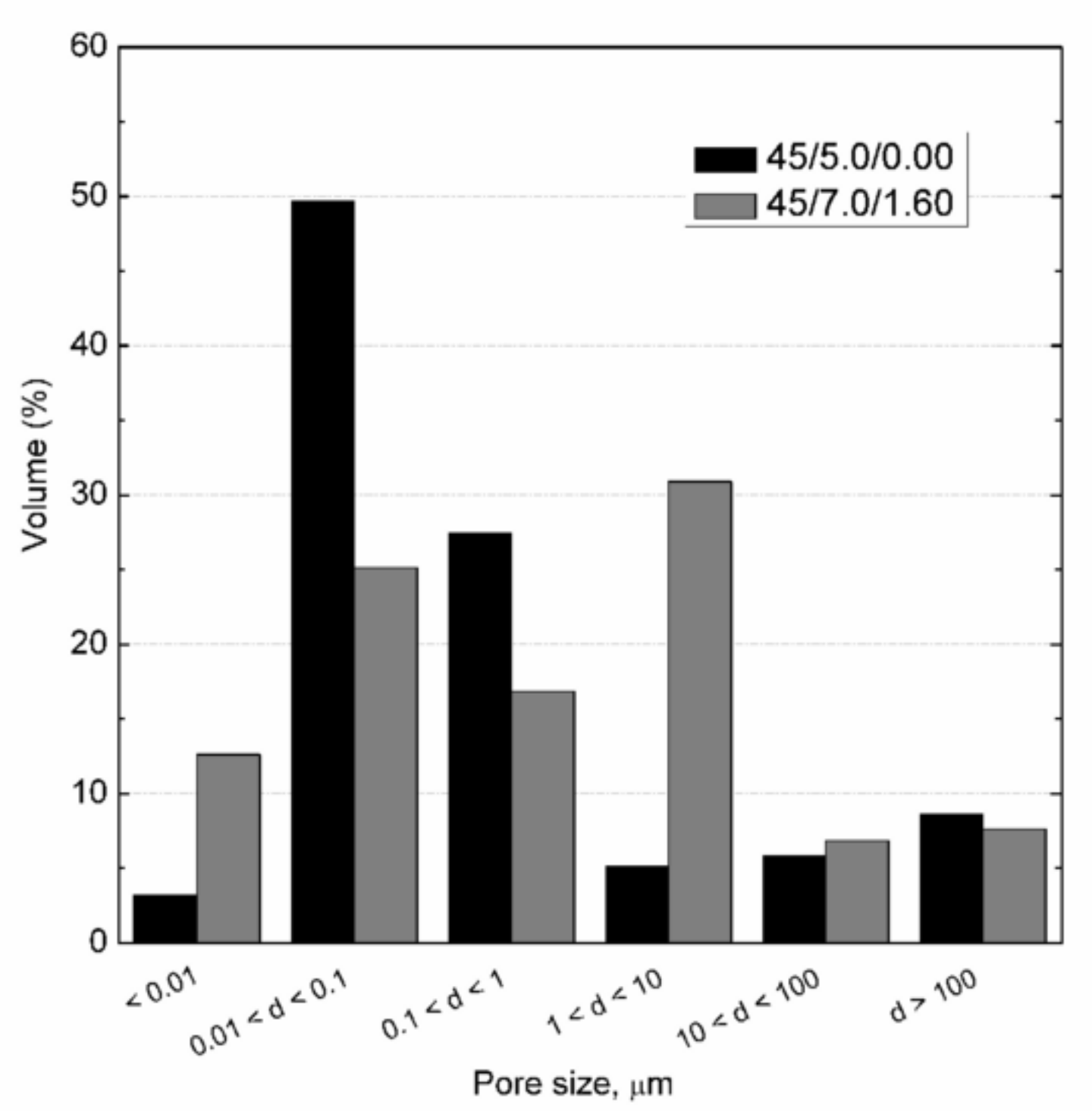

Figure
Click here to download high resolution image

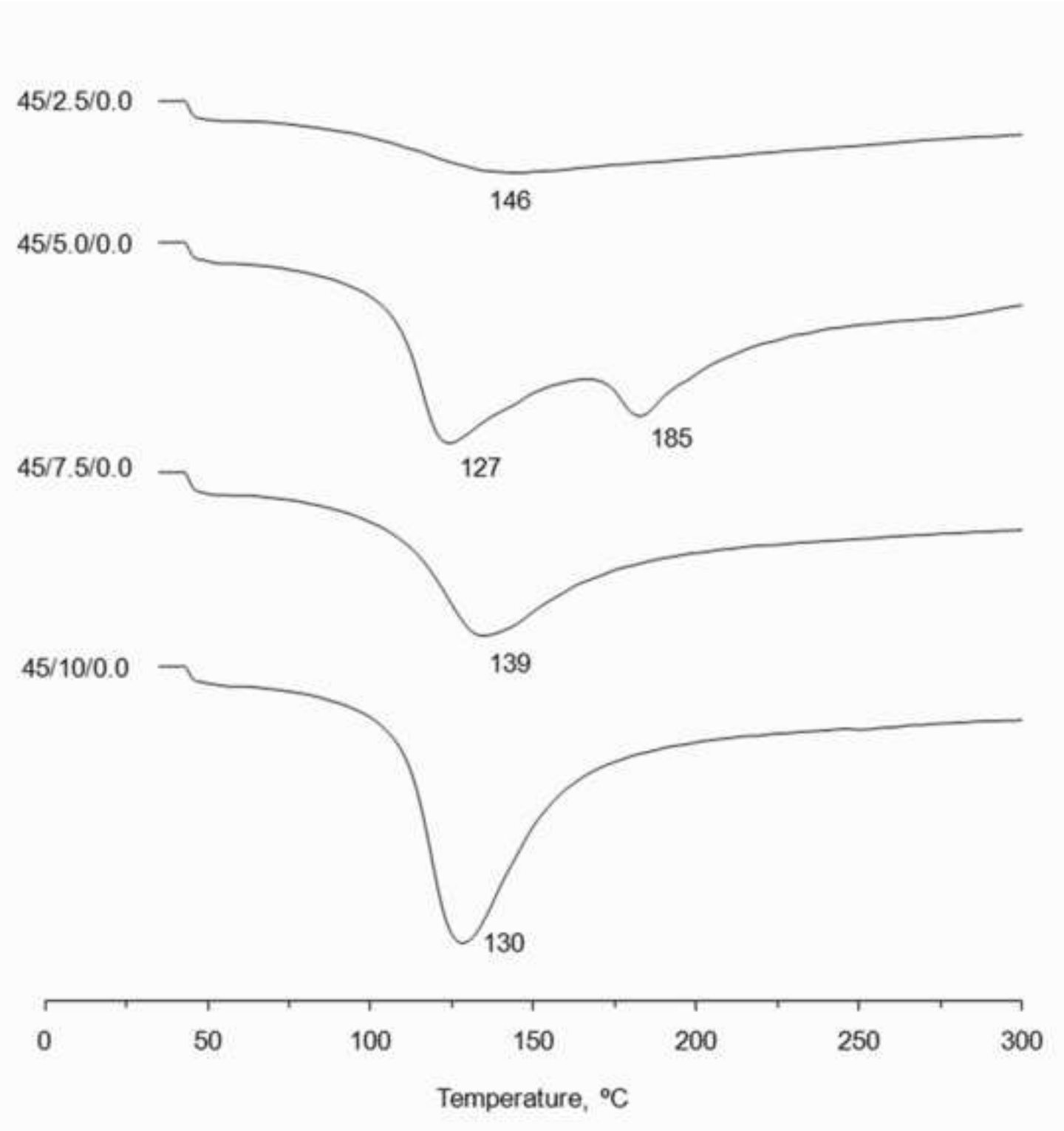

Figure
Click here to download high resolution image

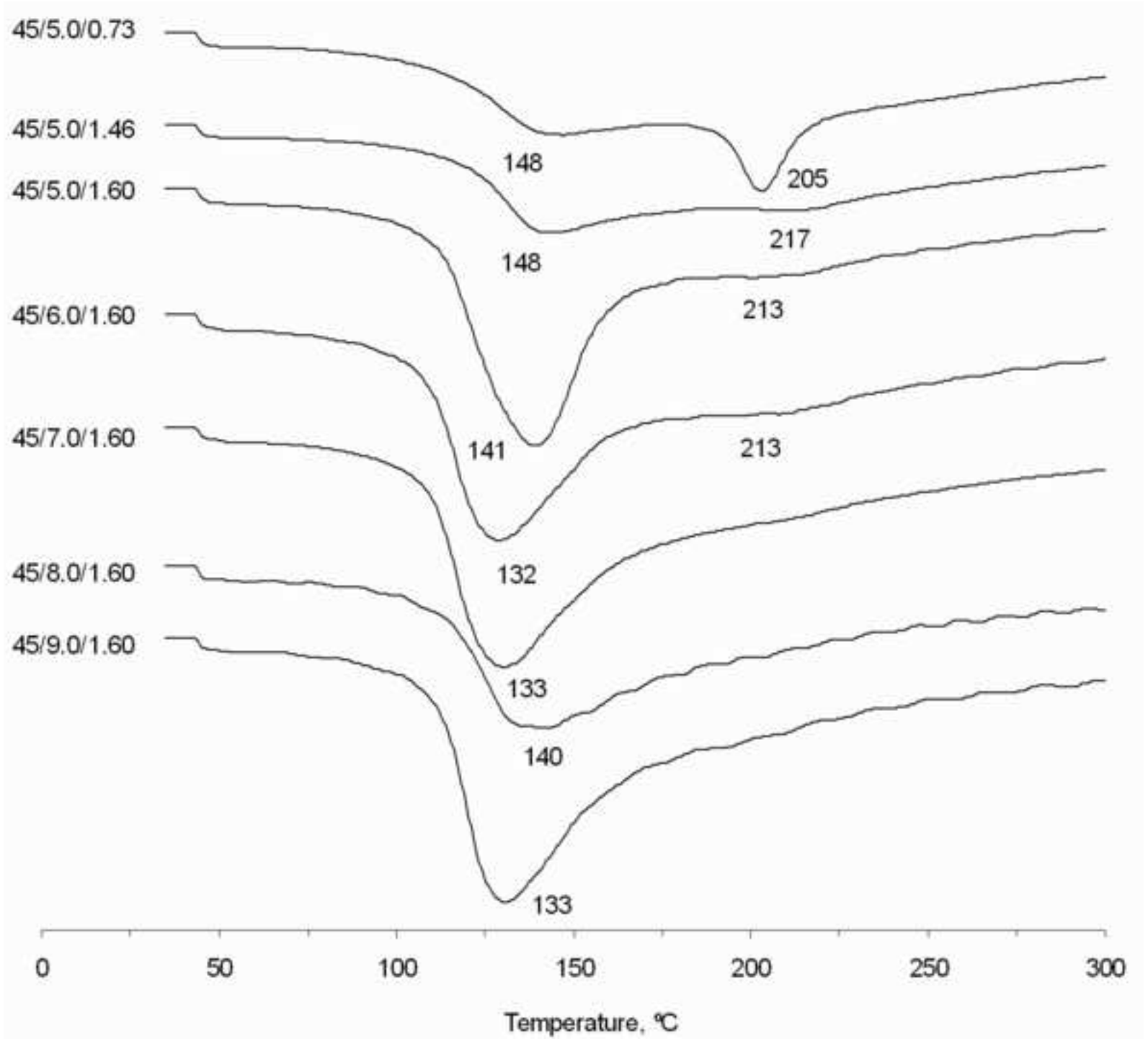

Figure
Click here to download high resolution image

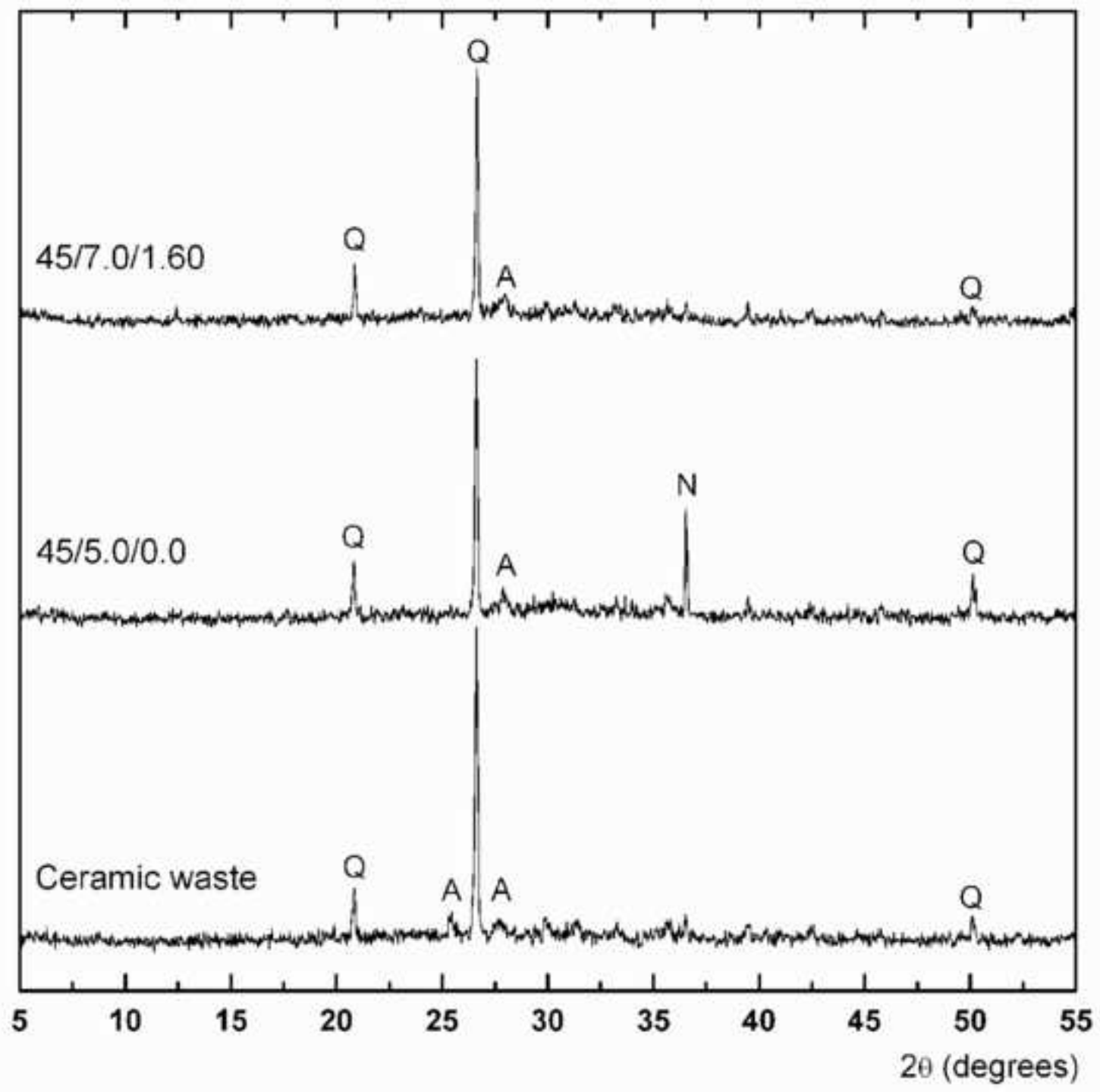

Figure

Click here to download high resolution image

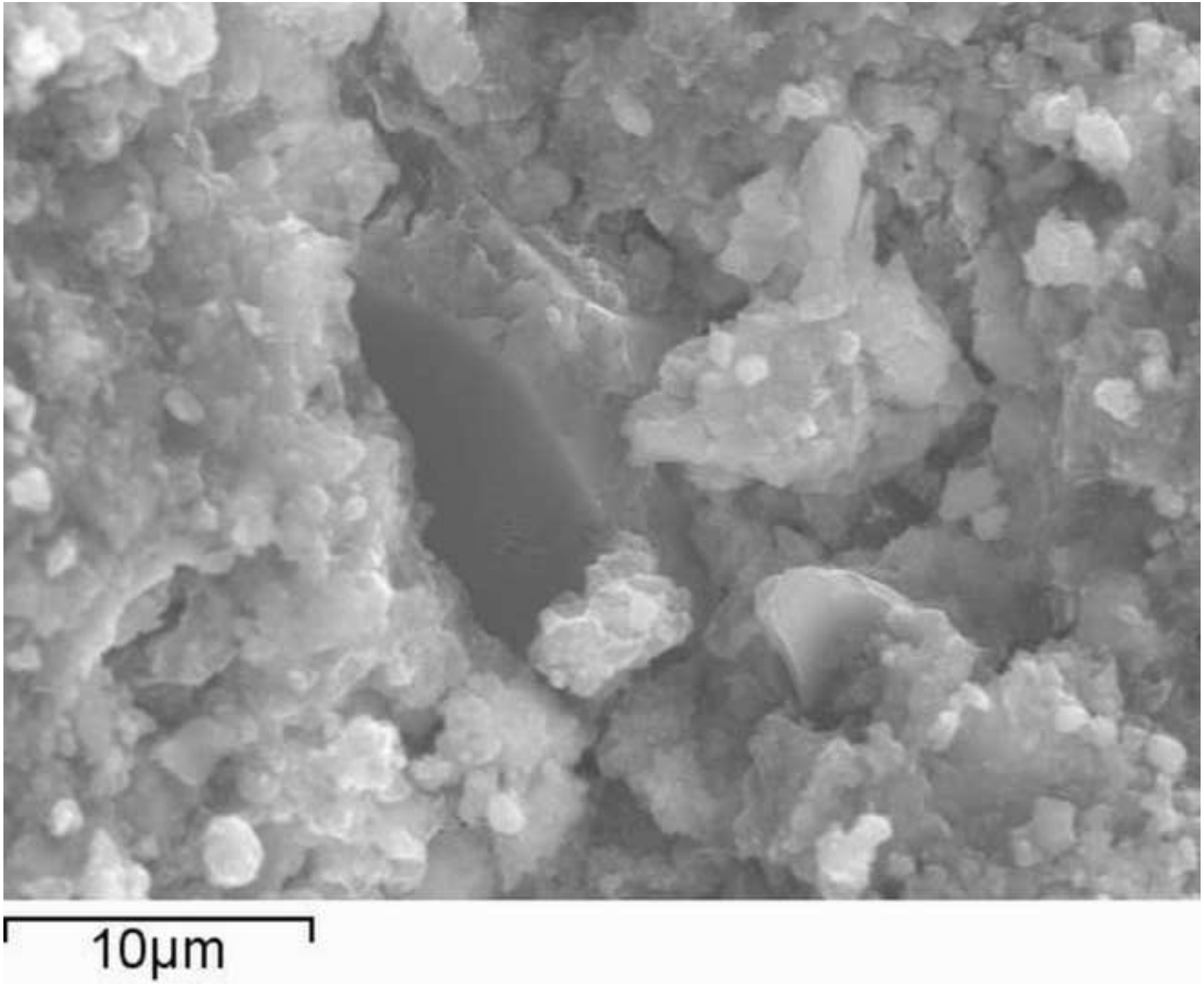

Figure

Click here to download high resolution image

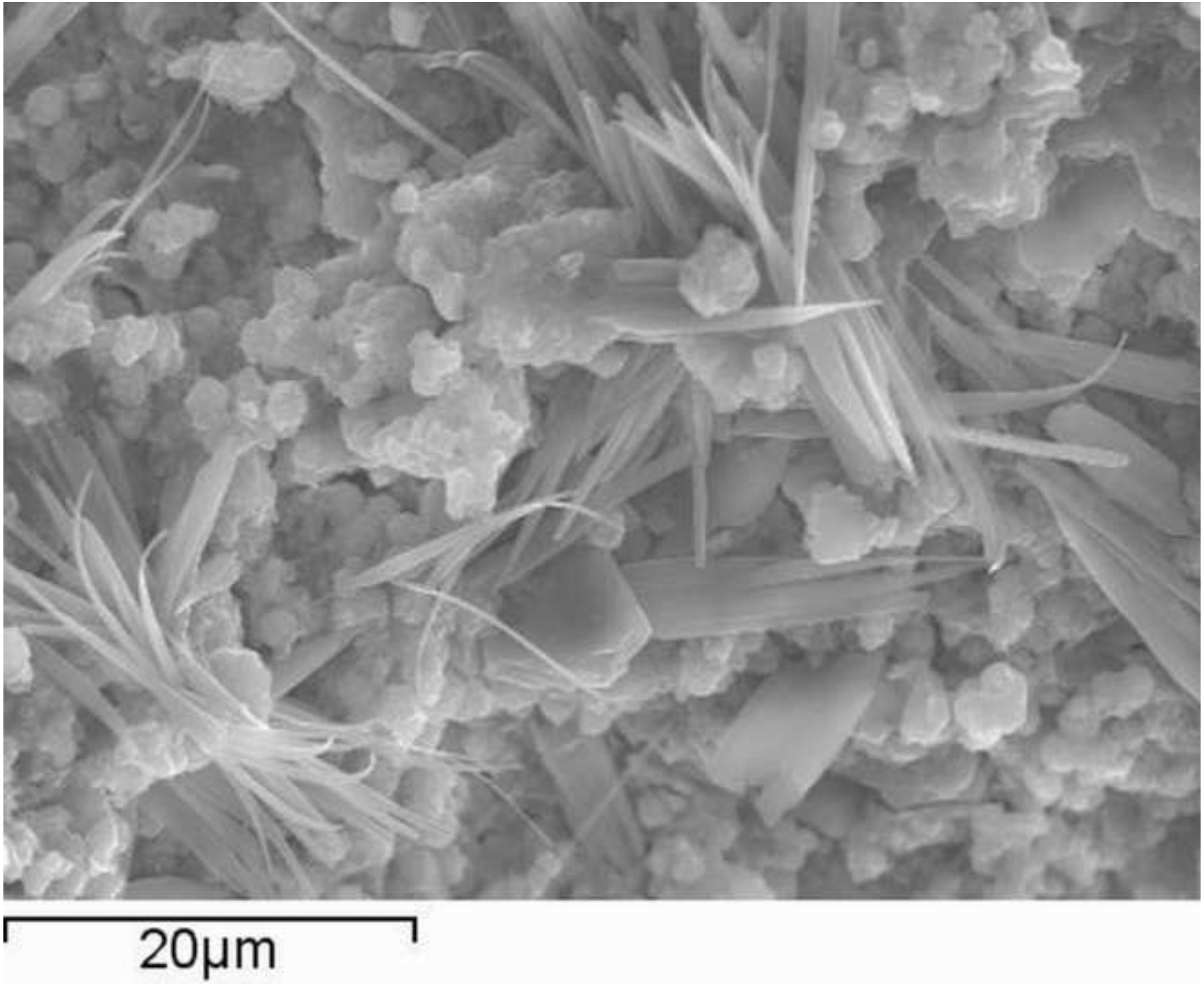

Figure

Click here to download high resolution image

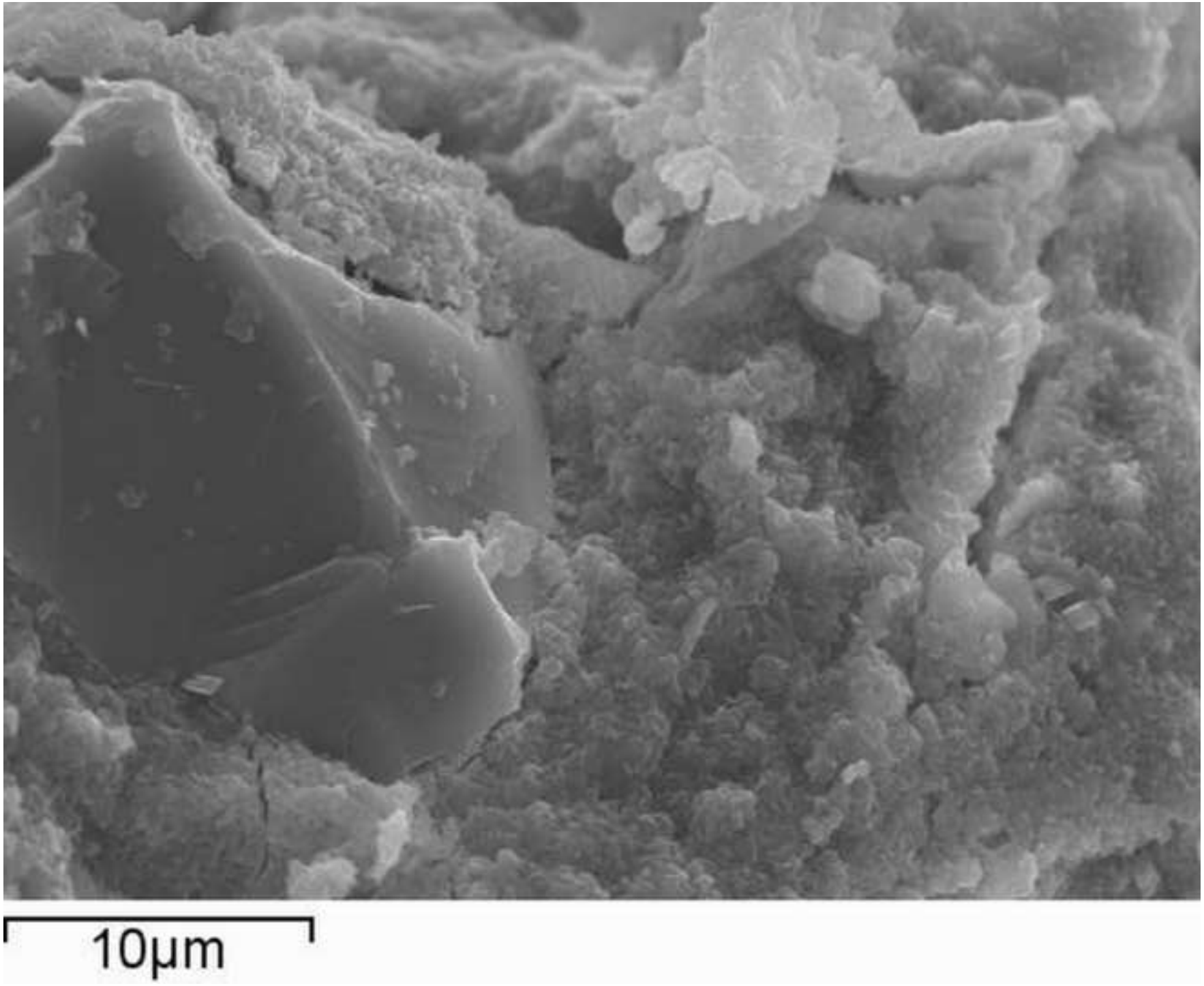

Figure

Click here to download high resolution image

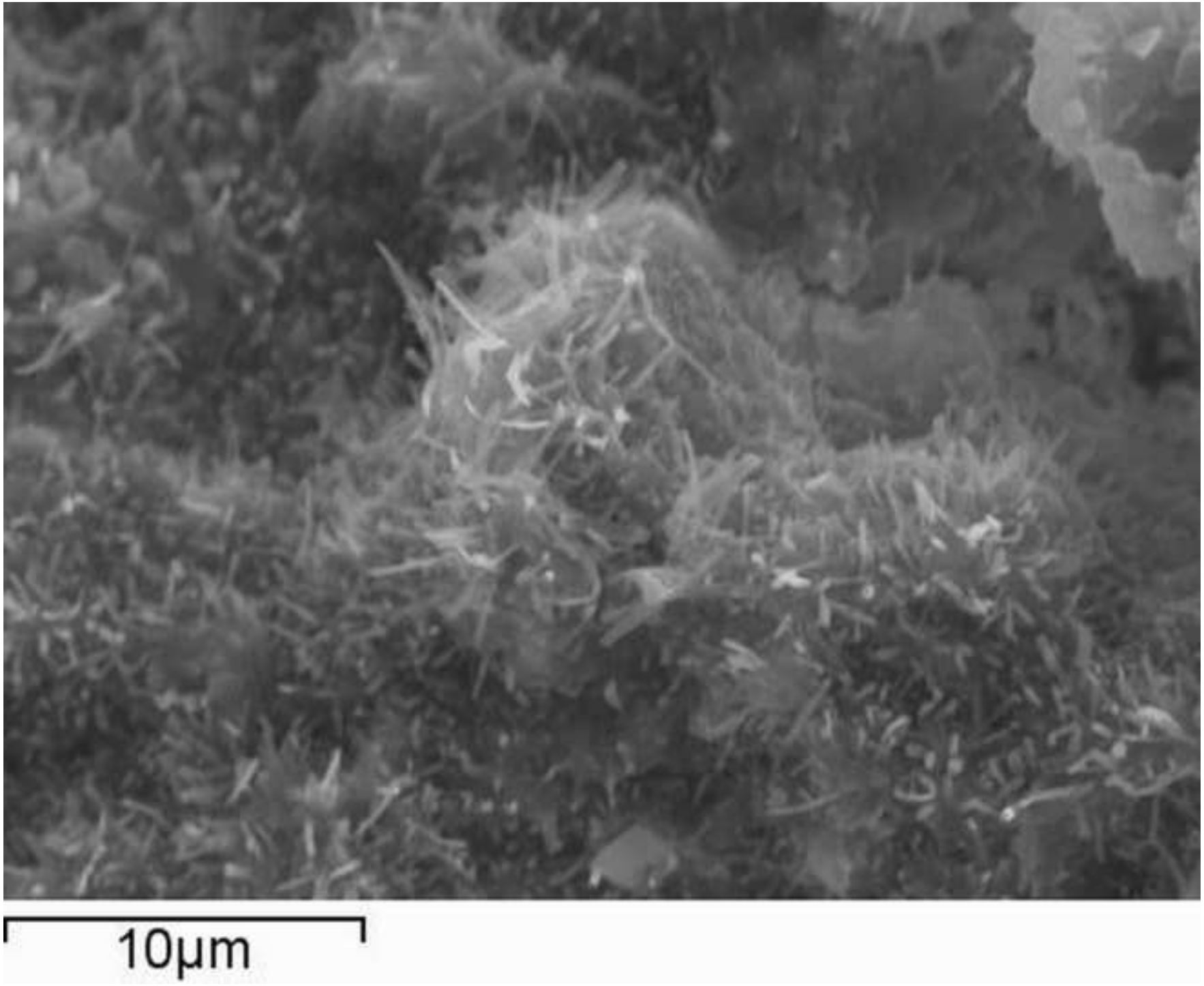

Figure

Click here to download high resolution image